Influence of pH and temperature on alunite dissolution: rates, products and insights on mechanisms from atomistic simulation

Patricia Acero[1],*, Karen A. Hudson-Edwards[1] and Julian D. Gale[2]

[1]Department of Earth and Planetary Sciences, Birkbeck College, University of London, Malet Street, London WC1E 7HX, UK

[2]Nanochemistry Research Institute/Curtin Institute for Computation, Department of Chemistry, Curtin University, P.O. Box U1987, Perth 6845, WA, Australia

*corresponding author: patri.acero@gmail.com

1

Abstract

The processes, rates, mechanisms, controlling factors and products of alunite ($KAl_3(SO_4)_2(OH)_6$) dissolution were assessed using batch dissolution experiments at pHs of c. 3, 4, 4.6, 7 and 8, and temperatures of c. 280, 293 and 313 K. Alunite dissolution is roughly congruent at pH 3, while at pH $\geq$ 3.9 the process is incongruent, giving a lower Al/K ratio in solution than in the pristine alunite sample. The decrease in the Al/K ratio appears to be caused by precipitation of secondary aluminium sulfate/hydroxysulfate minerals coating the surface of the dissolving alunite, as inferred from SEM images and XPS determinations, but these minerals do not passivate the alunite surface for the time frame of the experiments (up to 400 h). The lowest dissolution rates are obtained for pH 4.6 and 280 K. Both the temperature increase and any pH variation from that point lead to faster dissolution rates.

Based on the potassium release to solution, the influence of pH and temperature on the alunite dissolution rate for pH of 4.8 and below can be expressed as;

$$rate_K = 10^{-4.4\pm0.5} a_{H^+}^{0.10\pm0.02} e^{-32\pm3/RT}$$

Where $rate_K$ is the alunite dissolution rate (in mol·m⁻²·s⁻¹); is the activity of hydrogen ions in solution; R is the Universal gas constant (in kJ·mol⁻¹·K⁻¹) and T is temperature (in K).

For pH of 4.6 and above, the alunite dissolution rate can instead be expressed as;

$$rate_K = 10^{-2.5\pm0.8} a_{OH^-}^{0.14\pm0.02} e^{-39\pm4/RT}$$

where a_{OH^-} is the activity of hydroxyl ions in solution.

In light of the calculated values for the activation energy under the two sets of pH conditions (32±3 and 39±4 kJ·mol⁻¹), alunite dissolution appears to be surface-controlled. Examination of the most stable solvated alunite surfaces obtained by atomistic computer simulations suggests that the least energetically favourable steps during alunite dissolution are the detachment of either Al atoms or SO_4 tetrahedra from exposed surfaces. Thus, these processes are most probably the rate-determining steps in alunite dissolution.

Keywords

1. INTRODUCTION

The mobility of aluminium in low-temperature environments is generally very limited due to the low solubility of aluminium-containing mineral phases under circumneutral pH conditions (Nordstrom, 1982). However, dissolved aluminium may be one of the main elements present in areas affected by acid drainage, in poorly-buffered lakes receiving acid rain and in the pore-water of acid sulfate soils (Nordstrom, 1982). In these environments, dissolved aluminium plays a key role because it influences pH buffering and the mobility of other elements (Munk et al., 2002; Nordstrom, 2011). Moreover, high concentrations of aluminium may have severe effects on ecosystems (especially as a gill toxicant on fish; Birchall et al., 1989; Gensemer and Playle, 1999 and references therein, and causing growth inhibition of plants; Poschenrieder et al., 2008 and references therein; Matsumoto & Motoda, 2012). Some studies even suggest that aluminium may have negative effects on human health (e.g., Alzheimer's disease; Flaten, 2001). Thus, the knowledge of the factors controlling aluminium mobility in these sulfate-rich acid environments is of paramount importance to accurately assess the impact of dissolved aluminium on their aqueous geochemistry and ecology.

The behaviour of aluminium in systems such as those described above is commonly determined, at least partially, by the dissolution of aluminium sulfate minerals including alunite ($KAl_3(SO_4)_2(OH)_6$) (Jones et al., 2011). Alunite is present in weathered profiles, intertidal marine environments, lacustrine environments, magmatic-hydrothermal environments and metamorphic rocks (Stoffregen et al., 2000 and references therein). Furthermore, alunite is ubiquitous in acid mine environments (Nordstrom, 2011) and its presence has also been suggested in acid sulfate soils (Adams & Rawajfih, 1977; Prietzel & Hirsch, 1998; Delfosse et al., 2005; Prietzel & Mayer, 2005) and even for the surface of Mars (Swayze et al., 2008). While some previous studies have dealt with the dissolution kinetics of other similar sulfate minerals, such as jarosite (isostructural with alunite) (e.g. Smith et al., 2006a,b; Welch et al. 2008; Elwood Madden et al., 2012; Zahrai et al., 2013), the dissolution rates, products, reactions and mechanisms of alunite remain largely unknown. To the best of our knowledge, only partial results on the general trends of pH, temperature and brine effects on alunite dissolution have been reported previously (Miller et al., 2014; Elwood Madden et al., 2015).

To help bridge this gap, the kinetics of alunite dissolution under conditions similar to those commonly found in low-temperature aquatic environments are assessed in this work. With this

aim, batch dissolution experiments at pH values between 3 and 8, and at temperatures between 279 and 313K, were carried out using pure synthetic alunite as a starting material. The evolution of dissolved concentrations and reacting solids during the experiments were monitored and interpreted together with geochemical modelling, mineralogical analyses and atomistic computer simulation. Rate expressions including the influence of pH and temperature were obtained, and possible dissolution mechanisms involved in alunite dissolution are discussed. This information will allow a better understanding of the role of alunite dissolution on aluminium mobility and a more accurate prediction of the processes and expected conditions in the wide variety of environments where alunite is present.

2. MATERIALS & METHODS

2.1. Analytical, mineralogical and other techniques

The dissolved concentrations of K, Al and S in all the solutions involved in this study were obtained via Inductively Coupled Plasma Optical Emission Spectrometry (ICP-OES) on a Varian 720-ES (axial configuration) using a simultaneous solid-state detector (CCD). Calibration with sets of five standards was performed and laboratory standards were also analysed after every 10 samples and any drift in the measurements (generally less than 4%) was corrected accordingly. The quantification limits for K, Al and S were determined to be 2.6, 3.7 and 3.1 μmol L^{-1}, respectively, and the concentrations of the three elements were determined in the same run.

X-ray diffraction (XRD) was carried out using an 'X'Celerator' position-sensitive detector with the X-ray tube operated at 40 kV and 30 mA. Data were collected over the 2θ range from 5° to 110°, with a collection time of 13 h.

Images of the initial solid, and of the samples after the dissolution experiments, were obtained from Au-coated powders by Scanning Electron Microscopy (SEM) using a JSM6480LV instrument, with an accelerating voltage of 7 kV, a spot size of 32 and a working distance of 7 mm in Secondary Electron mode.

The surface area of the alunite prior to dissolution was determined by the BET method (Brunauer et al., 1938) in a Beckman Coulter SA3100 surface area analyser using 5-point N$_2$ adsorption isotherms.

The composition of the alunite surfaces before and after the dissolution experiments was studied by X-ray Photoelectron Spectroscopy (XPS). XPS data were obtained using a Thermo Scientific K-Alpha instrument, which utilised a monochromated Al K_α X-ray source (E=1486.6 eV) and achieved spectral intensity >2.5 Mcps with FWHM of 1.0 eV on the Ag 3d 5/2 peak from a clean metal sample. X-rays were microfocused at source to give a spot size on the sample of 400 microns. The analyser was a double focusing 180 degree hemisphere with mean radius of 125 mm, run in constant analyser energy (CAE) mode. Typical pass energies were 50 eV. The detector was a 128 channel position sensitive detector.

The pH variations during the dissolution experiments were monitored using a Thermo Scientific Orion Star A121 pH meter equipped with an Orion Triode probe with automated temperature correction. The pH meter was calibrated and checked using the appropriate certified buffer solutions of pH 2, 4, 7 and 10.

2.2. Alunite synthesis procedure

Alunite used in the dissolution experiments was synthesised using a modification of the method of Lager et al. (2001). For the synthesis, 2.6 g of $Al_2(SO_4) \cdot 18H_2O$, 0.58 g of K_2SO_4 and 14 ml of double distilled water were heated in the oven at 463K for 95h in a Parr bomb fitted with a Teflon sleeve. After this time, the bombs were taken out of the oven, quenched, and the resulting synthetic mineral was washed for 1h with pH 3 hydrochloric acid, then rinsed with double distilled water and dried for 24h in the oven at 323K. The resulting solid was manually disaggregated to obtain a finely powdered mineral sample (particle size below 20 microns).

The purity of the obtained synthetic mineral phase was confirmed by XRD spectra obtained for the initial synthetic material showed a typical alunite diffraction pattern without any other peaks or significant background from other phases. The composition of the mineral sample was confirmed by ICP-OES after digestion with aqua regia of a portion of the synthetic solid. According to these analytical results, the synthesized solid corresponds to an almost perfectly stoichiometric alunite (K:Al:SO_4 molar ratio of 0.97:2.71:2)

2.3 Dissolution experiments

The effect of different pH values and temperatures on the dissolution rate and products of alunite dissolution was examined by means of batch stirred experiments. These experiments were carried out at pH values c. 3, 4, 4.6, 7 and 8 and at three different temperatures (around 280, 293 and 313 K;

see Table 1). The experiments at the two lowest temperatures were carried out in a controlled temperature room, whereas the experiments at c. 313 K were performed using a magnetic stirred heating plate. All the reported conditions were addressed by triplicate experiments performed to ensure the reproducibility of the results obtained.

For each of the dissolution experiments, approximately 100 mg of the initial synthetic alunite were obtained by splitting and placed in a 250 mL glass beaker (slightly bottom-rounded) containing 200 mL of the target solution that is stirred at 400 rpm at the desired temperature. All the solutions were prepared using double distilled water (<18 $M\Omega \cdot cm^{-1}$). Solutions for pH below 4 were prepared by adding the required amounts of concentrated ultrapure H_2SO_4. For the experiments at a pH 4.6 and 4.8, double distilled water was used as the initial solution and the pH was allowed drifting freely, reaching the reported value in the first few hours of dissolution. The experiments at pH around 7 and 8 were carried out using a 0.005 M Tris solution at the target temperature buffered to the reported pH by adding the required amounts of 0.1 M HCl.

Stirring of the mixed mineral-solution was achieved using magnetic stirrers. Different stirring rates and bar types were tested during preliminary experiments to ensure that the reacting alunite samples were kept homogeneously suspended during the experiments. Octagonal stirring bars (length 41mm and diameter of 8mm), encapsulated in inert PTFE and pivoting on a ring were finally selected to ensure homogeneous suspension and to minimize the grinding of the synthetic sample during the experiments.

The variations of pH and temperature in the reacting solutions were monitored by regular measurements Additionally, the pH variations in blank solutions (without any reacting alunite) of the same composition and temperature as the ones used in the dissolution experiments were also monitored and K concentrations were determined in sampled aliquots, which proved that K release from the pH probe was negligible (below the quantification limit) under the described experimental conditions.

During the dissolution experiments, 4 mL aliquots of the reacting suspension were sampled every 5 to 48 h, filtered through disposable syringe filters with a pore size of 0.2 μm and immediately acidified with ultrapure concentrated HNO_3, before storing them refrigerated for analysis of the Al, K and S concentrations by ICP-OES. Sulfur concentrations in the sampled solutions are reported below as dissolved sulfate because this is the main stable species under the experimental conditions.

Speciation-solubility calculations using the experimental pH and temperature conditions and the measured concentrations of Al, K and S during the batch dissolution experiments were carried out using the PHREEQC code (Parkhurst and Appelo, 2013) and the wateq4f.dat (Ball and Nordstrom, 1991) thermodynamic database distributed with the code.

Preliminary tests proved that eight 4 mL suspension aliquots, sampled at intervals of 20 to 48h, were generally enough to determine the initial dissolution rates while being at the same time under far-from-equilibrium conditions with respect to alunite. Some of the experiments were kept running for up to 400h and the variations in the obtained results were negligible. After the dissolution experiments, stirring was stopped and the suspension was immediately filtered through a pore size of 0.2 μm, to obtain the remaining reacted alunite, which was dried at room temperature and stored in PET vials for SEM and XPS determinations.

2.3 Atomistic computer simulations

Atomistic computer simulations were performed using the GULP code (Gale and Rohl, 2003). Calculations are based on the Born model of solids that uses a combination of electrostatics and interatomic potentials to describe the energy of a system in terms of the atomic coordinates. In the case of ionic solids, the dominant term is the long-range Coulomb interaction, which is evaluated using an Ewald or Parry summation in the present work for the case of the bulk and surfaces, respectively. This is supplemented with short-range repulsive forces and, in the case of oxygen-oxygen interactions, with van der Waals attraction, as described by a Buckingham potential. A cut-off of 12 Å is applied to the short-range potentials. For the sulfate and hydroxyl anions a molecular description was used in which the intramolecular interactions are Coulomb-subtracted and the bonds modelled using a Morse potential. In the case of sulfate, a three-body angle-bending term was included to maintain the tetrahedral geometry. Parameters for the interatomic potentials for most interactions were taken from Smith et al. (2006), while the interactions for Al-O1/O2 were fitted to the structure of alunite. The full set of parameters used is reported in Table S1 (Electronic Supplementary Material).

Simulations are carried out using a standard Newton-Raphson energy minimization scheme with BFGS-updating of the exact inverse Hessian, which is explicitly re-calculated every 10 steps. Properties are then computed from the analytical second derivatives with respect to atomic coordinates and strain. For surface calculations, the optimized bulk structure was used to generate all relevant non-dipolar surface terminations as a function of (*hkl*) and cleavage plane shift using

the program GDis (Fleming and Rohl, 2005). Here a two-region approach was used in which region 1 is allowed to fully relax, while region 2 is held fixed at the bulk configuration in order to generate the potential due to the bulk acting on region 1. The thicknesses of both regions were increased until the surface energy was converged to better than 0.01 J/m^2.

In order to mimic the effect of aqueous solution at the surface of the crystal, the COSMIC solvation model (Gale and Rohl, 2007) was included. Here a dielectric continuum is placed at the solvent-accessible surface and charges are induced due to the electric field of the solid. The COSMIC method is based upon the COSMO solvation model (Klamt and Schüürmann, 1993), but with the additional constraint that the charge on the solvent-accessible surface must be fixed at an integer value such that the periodic system remains charge neutral. In this work the dielectric constant of the solvent was set to 78.4 for water, the radius for water was taken as 1.2 Å with an equal shift after construction of the solvent accessible surface based on 110 points per surface atom. The radii for the atoms were determined by fitting to the solvation free energies of the corresponding ions taken from the literature (Marcus, 1991). The final values were 2.01, 1.49683, 1.3551 and 2.3099 Å for H, O, Al and K, respectively.

2.4 Dissolution rates and rate equations

Dissolution rates were obtained from the slope of the linear fit to the measured concentrations vs time for each dissolution experiment. Rates were normalised with respect to the initial surface area of the synthetic alunite. Rate equations were obtained by fitting the experimental dissolution rates (in logarithmic form) as a function of pH and temperature by multiple linear regression. The significance of the fitted parameters was verified by using t-tests and the fitting residuals were carefully examined to ensure the absence of statistical outliers in the dataset.

3. RESULTS AND DISCUSSION

3.1 Evolution of Al, K and S dissolved concentrations throughout the dissolution experiments

The main results obtained in the dissolution experiments are detailed in Table 1. The experiments lasted for 10 to 15 days depending on the experimental conditions and, during this period of time, between 8 and 11 suspension aliquots were taken. During the dissolution experiments, the release of Al and K from the dissolving alunite to solution generally followed a constant rate after a few

hours and throughout the whole experimental runs (up to 390 h). For calculations of dissolution rates, dissolved concentrations of Al, K and S were corrected by subtracting the concentrations in the first suspension aliquot, taken a few hours after the beginning of the experiment. For the experiments presented in this study, the analytical concentrations in that first aliquot typically represented less than 30% of the concentrations for each element at the end of the experiment. This procedure, already used in earlier studies (e.g. Welch et al., 2008) allows the presence of any trace amount of labile solid to be corrected and the sulfate concentrations in the experiments carried out in H_2SO_4 solutions to be obtained. However, the uncorrected concentrations were retained for the speciation-solubility calculations.

As displayed in Fig. 1, there was a good linear correlation between the measured concentrations of both Al and K and the reaction time (R^2 mostly above 0.9 in the case of K, used for the calculation of the dissolution rates). A similar trend is also displayed by sulfate contents in most of the experiments. However, the large sulfate concentrations in some of the initial solutions (notably at pH 3) implied that the amount of sulfate released by alunite dissolution was only a small fraction of total dissolved sulfate. In these cases, the estimated dissolved sulfate concentrations were strongly influenced by the analytical uncertainty and, therefore, any linear trend for dissolved sulfate vs. time was not clearly observed. The dissolved mass of alunite during the dissolution experiments, estimated from K concentrations and using the initial stoichiometry of the synthetic alunite, represents less than 5% of the initial alunite mass in all the experiments.

For the experiments at pH around 3, alunite dissolution seems to be an almost congruent process (i.e., dissolved Al/K molar ratios close to 3, the value in alunite). In contrast, dissolution appears to be clearly incongruent (i.e. dissolved Al/K molar ratios lower than 3) for the experiments at pH 3.9 and above (Table 1). Thus, alunite dissolution rates may be better approached based on the rate of K release, as being more representative of the rate of alunite destruction than Al release. A similar approach has been adopted in earlier works focused on the dissolution of jarosite (isostructural with alunite) for similar reasons (e.g., Welch et al., 2008; Elwood Madden et al., 2012). In any case, this issue is addressed further below with the assistance of speciation-solubility calculations and the XPS results.

3.2 Evolution of pH values during dissolution

With regard to the pH evolution, measured pH values throughout the dissolution experiments at pH below 4 remained within ± 0.05 of their original value. In contrast, for the experiments carried

out using double distilled water as the target solution, the initial pH was around 5.5 and this value dropped to values below 5 within the first few hours of reaction with alunite, achieving the reported value in the first few hours of experiment and remaining within ± 0.1 pH units from that value throughout the experiments. Preliminary experiments carried out using NaOH solutions at pH 7 and 8 showed a pH decrease to values below 6.5 in the first few hours of interaction. For those pH values, the reported results correspond to Tris-buffered solutions, which led to pH values that remained within ±0.1 of their original value throughout the experiments.

3.3 Alunite dissolution rates

As displayed in Table 1, the obtained alunite dissolution rates range between $10^{-9.8}$ and $10^{-10.9}$ mol·m^{-2}·s^{-1}, with the lowest values corresponding to the experiments at 280 K and pH 4.6, and the highest to the experiments at 313 K and pH 8. These rates are between the values reported for jarosite by Elwood Madden et al. (2012) and Welch et al. (2008) and are roughly similar to those reported for alunite by Miller et al. (2014) (Table 1).

Alunite dissolution rates display a V-shaped trend when plotted vs. pH variations, with the lowest rates around pH 4.6-4.8 and increasing from that value with either an increase and decrease in pH (Fig. 2). A very similar trend has also been described for jarosite in earlier studies (Elwood Madden et al., 2012; Zahrai et al., 2013) and also for other mineral groups ranging from silicate phases to sulfide minerals (Chou and Wollast, 1985; Gislason and Oelkers, 2003; Lowson et al., 2005; Acero et al., 2007) and is usually related to changes in the dissolution mechanisms. Therefore, different linear rate expressions are proposed for the two pH ranges for alunite dissolution results in this study.

For pH values of 4.8 and below, the alunite dissolution rate expression obtained by multiple linear regression of the experimental rates is;

$$rate_K = 10^{-4.4 \pm 0.5} a_{H^+}^{0.10 \pm 0.02} e^{-32 \pm 3/RT} \qquad (1)$$

where *rate*$_K$ is the alunite dissolution rate, based on the release of K (in mol·m^{-2}·s^{-1}); is the activity of hydrogen ions in solution; *R* is the Universal gas constant (in kJ·mol^{-1}·K^{-1}) and *T* is temperature (in K).

For pH of 4.6 and above, alunite dissolution rate can be expressed as:

$$rate_K = 10^{-2.5\pm0.8} a_{OH^-}^{0.14\pm0.02} e^{-39\pm4/RT} \qquad (2)$$

where a_{OH^-} is the activity of hydroxyl ions in solution.

As shown in equations (1) and (2), the values of the activation energies, which represent the dependence of alunite dissolution rates on temperature, are approximately 32 and 39 kJ·mol⁻¹ for pH values below and above 4.6-4.8, respectively. These values are lower than that proposed by Elwood Madden et al. (2012) for jarosite (79 kJ·mol⁻¹), but are still higher than the values usually considered to correspond to diffusion-controlled dissolution kinetic mechanisms (less than around 20 kJ·mol⁻¹; Lasaga, 1981, 1998). Thus, alunite dissolution kinetics seems to be surface-controlled in light of the obtained activation energy values.

3.4 Speciation-solubility calculations with the experimental solutions

Speciation-solubility calculations using the compositions of the terminal slurries show that most of the solutions at pH 3.9 and above are close to equilibrium or supersaturated (Table 2) with respect to different aluminium hydroxides (diaspore; $AlOOH$, gibbsite; $Al(OH)_3$ and even felsobanyaite; $Al_4(SO_4)OH_{10} \cdot 5H_2O$) or amorphous aluminium hydroxide; $Al(OH)_3(a)$). For the experiments at pH 3.9, terminal slurries appear to be undersaturated with respect to all the aluminium phases listed, but they are very close to equilibrium with diaspore (Table 2) and, therefore, some precipitation of this phase cannot be completely ruled out. According to these calculations, equilibrium with respect to diaspore seems to be attained in the first few hours of dissolution for all the reported experiments at pH above 4.6 and the same applies for equilibrium with respect to gibbsite in all the experiments at pH above 4.8. Therefore, precipitation of these phases could explain, at least partially, the deficit of dissolved aluminium in the experiments clearly displaying incongruent dissolution.

In contrast, the calculated saturation indices for the experiments at pH around 3 indicate that those solutions are clearly undersaturated with respect to the same aluminium secondary phases (Table 2). Thus, their precipitation does not seem to be favoured from a thermodynamic point of view, which is consistent with the dissolved Al/K molar ratio (around 3 and roughly similar to the one in alunite) observed for those conditions.

With regard to the speciation in the target solutions (Table 3), K and sulfate are predominantly present as dissolved K^+ and SO_4^{2-}, respectively, for the whole range of studied pH and temperature values. In contrast, the speciation of dissolved Al tends to vary strongly depending on pH. As

displayed in Table 3, whereas Al^{3+} is the predominant species in the experiments at pH below 5, $Al(OH)_4^-$ is the main species (more than 85% of total dissolved aluminium) in the experiments at pH 7 to 8. Another interesting change in aluminium and sulfate speciation is the progressive increase of the $AlSO_4^+$ species with decreasing pH from pH 4.8 to pH 3 (Table 3). These changes in aqueous speciation and saturation states are discussed in relation to the dissolution reactions and mechanisms in the following sections.

3.5 XPS and SEM results and implications for secondary products of alunite dissolution

The XPS results suggest that some of the final solids after the dissolution experiments are enriched in Al compared to the initial synthetic alunite and, therefore, they also display lower relative amounts of S and K (Fig. 3). This is the case for all the experiments at pH 4.6-4.8 and, especially, at pH 7 to 8. For these conditions, the Al concentrations at the alunite surface after the dissolution experiments are between 15% and 57% higher than in the pristine synthetic alunite. By contrast, the reacted alunite samples after the experiments carried out at pH around 3 and 4 display similar relative amounts of Al, S and K to the unreacted initial alunite, which suggest that their surfaces are not largely enriched in aluminium. These observations are roughly consistent and complementary to the observed Al/K stoichiometric ratios in solution for the same experiments, especially at pH values of 4.6 and above (Table 1). The combined interpretation of both lines of evidence suggest that the dissolution process under those conditions either releases K preferentially over Al or leads to the precipitation of some type of Al phase on the dissolving alunite.

Aluminium peaks in the XPS results of the reacted alunite samples tend to have a maximum at binding energies between 74.1 and 75.2 eV, being in most cases between 74.4 and 74.9 eV. Unfortunately, these ranges may be attributed to either Al-OH or $Al-SO_4$ bonds in several aluminium phases (Arata and Hino, 1990; He et al., 1993; Sherwood, 1998; Rotole and Sherwood, 1998). Thus, the nature of secondary phases cannot be definitively established based on the XPS data.

The visual appearance of the samples before and after the dissolution experiments, as viewed by SEM, is consistent with the XPS results, with the observations in the target solutions and with the results from geochemical modelling. The surface of alunite grains in both the initial and the reacted samples at pH 3 (Fig. 4a) and 4 is mostly clean. On the contrary, alunite grains after the experiments at pH 7 and 8 (Fig. 4b) are clearly covered by a secondary precipitate. Moreover, these

samples tend to appear as grain aggregates, which might be related to the presence of fresh precipitates on alunite surfaces. Interestingly, the precipitation of secondary aluminium phases does not seem to produce any passivation of alunite, as suggested by the constant rate of potassium release from the dissolving mineral throughout the whole experimental run (up to 400 h). This could be due to the porous and discontinuous nature of the precipitated surface coating, though it is not possible to further test this hypothesis with the information currently available.

3.4 Atomistic computer simulations of alunite surface structure

The alunite structure is similar to the rest of the minerals in the alunite supergroup (Hendricks, 1937). It is based on linear tetrahedral-octahedral-tetrahedral sheets (T-O-T) made up from Al atoms in slightly distorted octahedral coordination (with four hydroxyl groups in a plane and two sulfate oxygens at the apices) and sulfate tetrahedra (Menchetti and Sabelli, 1976; Hudson-Edwards and Wright, 2011 and references therein). Potassium ions are hosted in the large cavities created by the arrangement of Al atoms and hydroxyl and sulfate groups. Each K^+ is coordinated by six hydroxyl groups from the Al octahedra and six oxygen atoms common to Al octahedra and sulfate tetrahedra (Schukow et al., 1999; Zema et al., 2012).

For the atomistic simulations presented in this study, an initial bulk alunite structure was obtained by optimisation of the published data of Schukow et al. (1999). Then the surface energy under vacuum conditions of all the possible non-dipolar cuts of this structure, corresponding to different surface orientations, was calculated. This procedure allows the most stable surfaces for alunite to be obtained, corresponding to the lowest surface energy values. These surfaces are the ones expected to have a morphological expression in alunite crystal under vacuum conditions, at least from a thermodynamic point of view. Once these surfaces were selected, a surface solvation model was applied to them using the method described above. This allowed the surface energy of the thermodynamically most stable alunite surfaces under solvated conditions, roughly similar to the ones expected under aqueous solution conditions, to be calculated (see results in Table 4).

As shown in Fig. 5, the theoretical solvated morphology calculated for alunite grains results from the expression of four different groups of surfaces: (003), (2-10), (10-2) and (1-1-1). There are two parallel (003)-type surfaces, which correspond to the most stable configurations (i.e. lowest surface energy and stronger morphological expression; Fig. 5). For the (2-10), (10-2) and (1-1-1) surface types, which have higher surface energies and weaker morphological expressions, there are 4, 8 and 2 different surfaces, respectively. Owing to their lower relative stability compared to the (003)

surface, alunite dissolution is expected to take place predominantly at these higher energy surfaces.

A closer examination of the terminations found at the solid-solution interface for the (2-10), (10-2) and (1-1-1) surface types reveals that all of them tend to expose both hydroxyl groups and/or K^+ (Fig. 6). In contrast, Al^{3+} and sulfate tetrahedra always lie beneath the exposed surface and are protected by the K^+/OH^- layers (Fig. 6). Therefore, alunite dissolution should proceed firstly by the detachment of the topmost K^+ and OH^- and, only then, by the release of Al^{3+} and SO_4^{2-}. Even in the case of the (2-10) surface, which displays a plane of 1 K^+ and 3 Al^{3+} approximately at the same depth under a top layer of hydroxyl groups (Fig. 6a), the removal of K^+ would be favoured by its smaller charge. In fact, the larger charge of both Al^{3+} and sulfate ions also supports the hypothesis that the kinetics of alunite dissolution may be determined by the detachment of these components from the surface terminations.

3.5 Overall dissolution reactions and dissolution mechanisms

The results from different pH values spanning between 3 and 8 in this study show that alunite dissolution rates are slowest at pH values around 4.6-4.8 and accelerate with both increases and decreases in pH from those conditions. This suggests that two different dissolution reactions and mechanisms may be taking place; one for pH below c. 4.6 and the other for higher pH values.

Alunite dissolution is almost congruent at pH around 3. Dissolution under these conditions does not seem to lead to the formation of detectable amounts of any secondary product precipitating on the alunite surface, according to the SEM (Fig. 4) and XPS results (Fig. 3), which is consistent with the speciation solubility calculations (Table 2). Thus, a plausible overall reaction expressing alunite dissolution around this pH is simply:
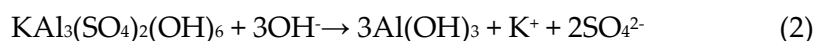
$$KAl_3(SO_4)_2(OH)_6 \rightarrow K^+ + 3Al^+ + 2SO_4^{2-} + 6OH^- \qquad (1)$$
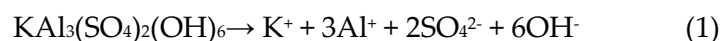
This reaction would lead to the release of 6 moles of OH^- for each mole of dissolved alunite. Therefore, alunite dissolution under unbuffered conditions within this pH range could lead to a pH increase, which is not observed throughout our experiments. In order to check the possible pH drift that alunite dissolution should produce under the experimental conditions presented here, some reaction-path calculations have been performed using the PHREEQC code. In these calculations, alunite was simulated to dissolve at pH 3 until the solution compositions observed in the experiments were attained. The results obtained by these calculations show that the pH

changes produced by alunite dissolution under those conditions should be almost unnoticeable (less than 0.05), consistent with the experimental observations.

For pH values around and above 3.9, alunite dissolution seems to be incongruent, with a preferential release of K over Al to the surrounding solution. This is especially clear for the experiments at pH of approximately 4.6 and above, whose terminal solids showed, in the XPS measurements, a clear surface enrichment in Al compared to the pristine synthetic alunite before the experiments (Fig. 3). Furthermore, the presence of secondary precipitates is apparent in the SEM images of the same solids (Fig. 4b). These pieces of evidence point towards the existence of a coupled process of alunite dissolution and precipitation of secondary aluminium phases.

The results of speciation-solubility calculations (Table 2) suggest for these experiments the equilibrium or oversaturation of the experimental solutions with respect to various aluminium sulfate and hydroxysulfate mineral phases (e.g., diaspore, gibbsite and felsobanyaite). Thus, both alunite dissolution (reaction 1) and secondary precipitation of aluminium may take place in these cases, according to similar reactions to 2 and 3;

$$KAl_3(SO_4)_2(OH)_6 + 3OH^- \rightarrow 3Al(OH)_3 + K^+ + 2SO_4^{2-} \qquad (2)$$

$$4KAl_3(SO_4)_2(OH)_6 + 15H_2O + 6OH^- \rightarrow 3Al_4(SO_4)(OH)_{10} \cdot 5H_2O + 4K^+ + 5SO_4^{2-} \qquad (3)$$

for the precipitation of gibbsite/diaspore/amorphous aluminium hydroxide (reaction 2) and felsobanyaite (reaction 3). The precipitation of these aluminium phases would lead to the consumption of OH^-, which may lead to a decrease in pH. This is consistent with the observed decrease in pH during dissolution in the experiments using distilled water (initial pH of 5.5 and pH after alunite dissolution below 5) and in preliminary experiments using unbuffered solutions at pH 7 and 8. Moreover, such a pH decrease is also consistent with the results obtained by reaction-path calculations with the PHREEQC code to simulate the same processes.

For the experiments at pH around 4, the overall reaction might be similar to reaction 3. Even though the results for these conditions do not fully correspond to congruent dissolution (see Table 1), the precipitation of secondary aluminium phases does not seem to be as clear as in the case of the experiments at pH of 4.6 and above. Although alunite surfaces after the dissolution experiments do not show evidences of these processed neither by XPS (Fig. 3) nor by SEM, the precipitation of a secondary phase similar to diaspore cannot be ruled out, in the light of the speciation-solubility calculations (Table 2).

Taking into account the results obtained by atomistic computer simulations on the alunite structure, the thermodynamically favoured hypothesis for the rate-limiting process for alunite dissolution seems to be the detachment of either Al^{3+} or sulfate groups from the surface. As described in section 3.4, both ions tend to be protected from dissolution by outer layers of K^+ and hydroxyl groups in the energetically stable solvated surfaces.

4. CONCLUSIONS

In this study, the kinetics of alunite dissolution under similar pH and temperature conditions to those found in most natural systems has been examined using synthetic alunite by means of batch dissolution experiments at different pH values (between 2.9 and 8) and temperatures (between 279 and 313 K). The results provide some insight into alunite dissolution kinetics.

Alunite seems to dissolve incongruently for solutions at pH above or around 4, which may be attributed, at least partially, to the precipitation of secondary aluminium phases (Al-hydroxides and/or felsobanyaite). Interestingly, such surface changes do not lead to any apparent passivation of alunite. In contrast, alunite dissolution seems to be closer to congruent at pH around 3, leading to similar Al/K molar ratios in the reacting solutions and mineral phase.

Based on the potassium release during dissolution, the lowest alunite dissolution rates are obtained for pH 4.6 and 280 K. Both the temperature increase and any pH variation from that point lead to faster dissolution rates. Whereas the influence of pH variations seems to be very limited for both pH ranges (reaction orders below 0.15 with respect to the activity of eitherdissolved hydrogen ions or hydroxyl groups), the influence of temperature increase is more noticeable. The increase of temperature from 280 to 313 K results in a four- to six-fold increase in the alunite dissolution rate, corresponding to activation energies of 32±3 and 39±4 kJ·mol^{-1}·K^{-1} for the pH range below and above c. 4.6, respectively. These values point toward surface control of alunite dissolution.

Atomistic computer simulations suggest that alunite dissolution mechanisms and rates are probably controlled by the detachment of either Al atoms or SO_4 tetrahedra from mineral surfaces, which tend to expose K and OH groups in the topmost layers of the thermodynamically most stable solvated surfaces.

Two mathematical expressions (for pH below 4.8 and above 4.6) have been proposed to include the influence of pH and temperature on alunite dissolution rates. These expressions can be easily incorporated into geochemical and reactive-transport calculations and will hopefully allow a better prediction of the expected compositional evolution of low-temperature aqueous environments in contact with alunite, such as acid mine/rock drainage, acid sulfate soils, weathered profiles, intertidal marine environments or lacustrine environments, among many others.

Some questions related to alunite dissolution processes remain open and should be explored in future studies, such as the exact mineralogical nature of secondary precipitates and the structure of precipitated surface coatings, the influence of other types of solutions (e.g., higher ionic strength) on alunite dissolution rates or the influence on the dissolution rates, processes and mechanisms of different degrees of K^+ substitution by H_3O^+.

References

Acero, P., Cama, J., Ayora, C., 2007. Rate law for galena dissolution in acidic environment. Chem. Geol., 245(3), 219-229.

Adams, F., Rawajfih, Z., 1977. Basaluminite and alunite: A possible cause of sulfate retention by acid soils. Soil Sci. Soc. Am. J. 41(4), 686-692.

Arata, K., Hino, M., 1990. Solid catalyst treated with anion: XVIII. Benzoylation of toluene with benzoyl chloride and benzoic anhydride catalysed by solid superacid of sulfate-supported alumina. Appl. Catalysis 59(1), 197-204.

Ball J.W., Nordstrom D.K., 1991. User's manual for WATEQ4F, with revised thermodynamic database and test cases for calculating speciation of major, trace, and redox elements in natural waters. U.S. Geol. Surv. Open-File Rep. 91-183, p. 189.

Berner, R.A., 1981. Rate laws of chemical reactions. In: Lasaga, A.C., Kirkpatrick. R.J. (Eds.) Kinetics of Geochemical Processes. Mineralogical Society of America, Reviews in Mineralogy, 8; pp. 111-134.

Birchall, J.D., Exley, C., Chappell, J.S., Phillips, M.J., 1989. Acute toxicity of aluminium to fish eliminated in silicon-rich acid waters. Nature 338, 146-148.

Brunauer, S., Emmett, P.H., Teller, E., 1938. Adsorption of gases in multimolecular layers. J. Am. Chem. Soc. 60(2), 309-319.

Chou, L., Wollast, R., 1998. Steady-state kinetics and dissolution mechanisms of albite. Am. J. Sci., 285, 963–993.

Delfosse, T., Elsass, F., Delvaux, B., 2005. Direct evidence of basic aluminium sulphate minerals in an S-impacted Andosol. Eur. J. Soil Sci. 56(3), 281-286.

Elwood Madden, M. , Madden, A. S., Rimstidt, J. D., Zahrai, S., Kendall, M. R., Miller, M. A., 2012. Jarosite dissolution rates and nanoscale mineralogy. Geochim. Cosmochim. Acta, 91, 306-321.

Elwood Madden, M. E., Elwood Madden, A. S., Miller, J. M., Phillips-Lander, C. M., Pritchett, B. R., 2015. Fluid alteration of alunite group minerals: comparing dissolution rates and products. Lunar and Planetary Science Conference 46, 1513.

Flaten, T.P., 2001. Aluminium as a risk factor in Alzheimer's disease, with emphasis on drinking water. Brain Res. Bull. 55(2), 187-196.

Fleming, S., Rohl, A., 2005. GDIS: a visualization program for molecular and periodic systems. Z. Krist. 220(5-6), 580-584.

Gale, J.D., Rohl, A.L., 2003. The general utility lattice program (GULP). Mol. Simulat. 29(5), 291-341.

Gale, J.D., Rohl, A.L., 2007. An efficient technique for the prediction of solvent-dependent morphology: the COSMIC method. Mol. Simulat. 33(15), 1237-1246.

Gensemer, R.W., Playle, R.C., 1999. The bioavailability and toxicity of aluminum in aquatic environments. Crit. Rev. Environ. Sci. Technol. 29(4), 315-450.

Gislason, S.R., Oelkers, E.H., 2003. Mechanism, rates, and consequences of basaltic glass dissolution: II. An experimental study of the dissolution rates of basaltic glass as a function of pH and temperature. Geochim. Cosmochim. Acta, 3817–3832.

He, H., Alberti, K., Barr, T. L., Klinowski, J., 1993. ESCA studies of aluminophosphate molecular sieves. J. Phys. Chem. 97(51), 13703-13707.

Hendricks, S.B., 1937. The crystal structure of alunite and the jarosites. Am. Min. 22, 773-784.

Hudson-Edwards, K.A., Wright, K., 2011. Computer simulations of the interactions of the (012) and (001) surfaces of jarosite with Al, Cd, Cu^{2+} and Zn. Geochim. Cosmochim. Acta 75(1), 52-62.

Jones, A.M., Collins, R.N., Waite, T.D., 2011. Mineral species control of aluminum solubility in sulfate-rich acidic waters. Geochim. Cosmochim. Acta 75(4), 965-977.

Klamt, A., Schüürmann, G., 1993. COSMO: A new approach to dielectric screening in solvents with explicit expressions for the screening energy and its gradient. J. Chem. Soc. Perkin Trans. 2, 799-805.

Lager, G.A., Swayze, G.A., Loong, C.K., Rotella, F.J., Richardson, J.W., Stoffregen, R.E., 2001. Neutron spectroscopic study of synthetic alunite and oxonium-substituted alunite. Can. Miner. 39(4), 1131-1138.

Lasaga, A.C., 1981. Rate laws of chemical reactions. In: Lasaga, A.C., Kirkpatrick. R.J. (Eds.) Kinetics of Geochemical Processes. Mineralogical Society of America, Reviews in Mineralogy, 8, 1-68.

Lasaga, A.C., 1998. Reaction kinetics in geosciences. Princeton University Press, Princeton, New Jersey, 811 p.

Lowson, R.T., Comarmond, M.C.J., Rajaratnam, G., Brown, P.L., 2005. The kinetics of the dissolution of chlorite as a function of pH and at 25 °C. Geochim. Cosmochim. Acta 69, 1687–1699.

Marcus, Y., 1991. Thermodynamics of solvation of ions. Part 5 – Gibbs free energy of hydration at 298.15 K. J. Chem. Soc. Faraday Trans. 87(18), 2995-2999.

Matsumoto, H., Motoda, H., 2012. Aluminum toxicity recovery processes in root apices. Possible association with oxidative stress. Plant Sci. 185, 1-8.

Menchetti S., Sabelli C., 1976. Crystal chemistry of the alunite series: crystal structure refinement of alunite and synthetic jarosite. Neues Jahr. Miner. Monatshefte 9, 406–417.

Miller, J.L., Elwood Madden, M.E., Elwood Madden, A.S., Pritchett, B.N., 2014. Temperature, pH, and brine Effects on alunite dissolution: implications for Mars. Lunar and Planetary Institute Science Conference Abstracts 45, 2344.

Munk, L., Faure, G., Pride, D.E., Bigham, J.M., 2002. Sorption of trace metals to an aluminum precipitate in a stream receiving acid rock-drainage; Snake River, Summit County, Colorado. Appl. Geochem. 17(4), 421-430.

Nordstrom, D.K., 1982. The effect of sulfate on aluminum concentrations in natural waters: some stability relations in the system Al_2O_3-SO_3-H_2O at 298 K. Geochim. Cosmochim. Acta, 46(4), 681-692.

Nordstrom, D.K., 2011. Mine waters: acidic to circumneutral. Elements 7, 393-398.

Parkhurst, D.L., Appelo, C.A.J., 2013. Description of input and examples for PHREEQC version 3: A computer program for speciation, batch-reaction, one-dimensional transport, and inverse geochemical calculations. US Geological Survey Techniques and Methods, book 6, chap. A43, 497 p.

Poschenrieder, C., Gunsé, B., Corrales, I., Barceló, J., 2008. A glance into aluminum toxicity and resistance in plants. Sci. Total Environ. 400(1), 356-368.

Prietzel, J., Hirsch, C., 1998. Extractability and dissolution kinetics of pure and soil-added synthesized aluminium hydroxy sulphate minerals. Eur. J. Soil Sci. 49(4), 669-681.

Prietzel, J., Mayer, B., 2005. Isotopic fractionation of sulfur during formation of basaluminite, alunite, and natroalunite. Chem. Geol. 215(1), 525-535.

Rotole, J.A., Sherwood, P.M., 1998. Gamma-alumina (γ-Al_2O_3) by XPS. Surf. Sci. Spectra 5(1), 18-24.

Schukow, H., Breitinger, D.K., Zeiske, T., Kubanek, F., Mohr, J., Schwab, R.G., 1999. Localization of hydrogen and content of oxonium cations in alunite via neutron diffraction. Z. Anorg. Allg. Chem. 625, 1047-1050.

Sherwood, P.M., 1998. Introduction to studies of aluminum and its compounds by XPS. Surf. Sci. Spectra 5(1), 1-3.

Smith, A. M., Dubbin, W. E., Wright, K., Hudson-Edwards, K. A. 2006a. Dissolution of lead-and lead–arsenic-jarosites at pH 2 and 8 and 20 C: Insights from batch experiments. Chemical Geology 229(4), 344-361.

Smith, A. M., Hudson-Edwards, K. A., Dubbin, W. E., Wright, K., 2006b. Dissolution of jarosite [$KFe_3(SO_4)_2(OH)_6$] at pH 2 and 8: Insights from batch experiments and computational modelling. Geochimica et Cosmochimica Acta 70(3), 608-621.

Stoffregen, R.E., Alpers, C.N., Jambor, J.L., 2000. Alunite-jarosite crystallography, thermodynamics, and geochronology. In: Alpers, C.N., Jambor, J.L., Nordstrom, D.K. (Eds.) Sulfate Minerals. Crystallography, Geochemistry, and Environmental Significance. Mineralogical Society of America, Reviews in Mineralogy and Geochemistry 40, pp. 454-479.

Swayze, G.A., Ehlmann, B.L., Milliken, R.E., Poulet, F., Wray, J.J., Rye, R.O., Clark, R.N., Desborough, G.A., Crowley, J.K., Gondet, B., Mustard, J.F., Seelos, K.D., Murchie, S.L., 2008. Discovery of the acid-sulfate mineral alunite in Terra Sirenum, Mars, using MRO CRISM: possible evidence for acid-saline lacustrine deposits? American Geophysical Union, Fall Meeting 2008, abstract #P44A-04.

Welch, S.A., Kirste, D., Christy, A.G., Beavis, F.R., Beavis, S.G., 2008. Jarosite dissolution II - Reaction kinetics, stoichiometry and acid flux. Chem. Geol. 254, 73-86.

Zahrai, S.K., Madden, M.E.E., Madden, A.S., Rimstidt, J.D., 2013. Na-jarosite dissolution rates: The effect of mineral composition on jarosite lifetimes. Icarus, 223(1), 438-443.

Zema, M., Callegari, A.M., Tarantino, S.C., Gasparini, E., Ghigna, P., 2012. Thermal expansion of alunite up to dehydroxylation and collapse of the crystal structure. Min. Mag. 76(3), 613-623.

TABLES AND FIGURES

Table captions

Table 1: Summary of results obtained in alunite dissolution experiments in this study and for alunite and jarosite dissolution experiments under similar conditions in earlier works (for comparison).

Table 2: Saturation indices in the final solutions from the different experimental conditions explored in this study with respect to the main possible aluminium secondary phases. Positive values correspond to theoretical oversaturation (precipitation thermodynamically favoured) and negative values indicate theoretical oversaturation (precipitation thermodynamically hindered).

Table 3: Distribution of Al, K and S dissolved species (in %) under the different conditions assessed in this study, as obtained from PHREEQC speciation-solubility calculations, showing the increasing proportions of dissolved $AlSO_4^+$ with the pH decrease from pH 4.8 and the large proportions of $Al(OH)_4^-$ at pH 7 and above.

Table 4: Summary of optimised energy values (in $J \cdot m^{-2}$) obtained for the more energetically favoured alunite surface both *in vacuo* and under solvation conditions. For some of the surfaces, more than one configuration is thermodynamically possible.

Table S1 (Electronic Supplementary Material): Force field parameters used in the atomistic simulation of alunite. Here O1 denotes an oxygen of a sulfate anion, while O2 is that of a hydroxyl group. All Buckingham potentials act intermolecularly with a cut-off of 12 Å, while Morse and three-body terms are intramolecular only. Charges for K, Al, H, O1 and O2 are +1, +3, +0.426, -0.84 and -1.426, respectively, with all molecules being Coulomb-subtracted.

Figure captions

Figure 1: Evolution of dissolved K and Al concentrations vs. time throughout a representative dissolution experiment (Tris-buffered pH 8 and 293K), typically displaying a linear trend from the start of the experiment. The calculated dissolution rate corresponds to the slope of the linear fit to this evolution.

Figure 2: Alunite dissolution rates (in logarithmic scales and based on potassium release) obtained in this study vs. pH and for different temperatures (a) and vs 1000/RT (b).

Figure 3: Summary of results obtained by XPS examination of the powdered alunite samples after the dissolution experiments. Elemental bars represent the proportion of Al, K and S in the surfaces on the reacted samples with respect to the same values in the pristine alunite samples. Positive and negative values correspond to increases and decreases of contents of the given element in the reacted surfaces compared to stoichiometric alunite, respectively.

Figure 4: SEM images of selected alunite samples after dissolution in solutions at pH 3 and 293 K (a), and at pH 8 and 313 K (b).

Figure 5: Theoretical morphology for a solvated alunite crystallite, as calculated by atomistic computer simulations. The size of the surfaces is proportional to their stability (i.e., lower surface energy). As displayed, there are only four types of symmetry inequivalent theoretical surfaces exposed.

Figure 6: Structure of the most stable theoretical solvated alunite surfaces (except (003)), as calculated by atomistic computer simulations: a) (2-10) surface; b) (10-2) surface, c and d) two different terminations of the (1-1-1) alunite surface.

Tables

Mineral	pH	T(K)	Solution type	Log Rate[1] $(mol \cdot m^{-2} \cdot s^{-1})$	Al/K solution ratio	Source
Alunite	2.9	280	H_2SO_4	-10.74	1.7-3	This study
Alunite	2.9	293	H_2SO_4	-10.39	2.0-2.7	This study
Alunite	3.2	312	H_2SO_4	-10.14	2-3.2	This study
Alunite	3.9	293	H_2SO_4	-10.52	1.7-2.4	This study
Alunite	4.6	280	Water[2]	-10.89	1.3-2.0	This study
Alunite	4.8	294	Water[2]	-10.62	0.8-1.4	This study
Alunite	7.0	293	Tris buffer	-10.25	0.1-0.7	This study
Alunite	7.8	279	Tris buffer	-10.59	0.5-0.8	This study
Alunite	8.0	294	Tris buffer	-10.19	1.5-2.7	This study
Alunite	8.0	313	Tris buffer	-9.79	1.3-2.1	This study
Alunite	8	not reported	Tris buffer	-11.0	-	Miller *et al.* (2014) [3]
Alunite	5	not reported	Water[2]	-11.3	-	Miller *et al.* (2014) [3]
K-Jarosite	3.1	296	H_2SO_4	-9.09	-	Elwood Madden *et al.* (2012)
K-Jarosite	3.9	296	H_2SO_4	-9.28	-	Elwood Madden *et al.* (2012)
K-Jarosite	4.4	296	Water	-9.20	-	Elwood Madden *et al.* (2012)
K-Jarosite	6.8	296	MES	-8.02	-	Elwood Madden *et al.* (2012)
K-Jarosite	7.8	296	NaOH	-6.60	-	Elwood Madden *et al.* (2012)
K-Jarosite	3.15	298	H_2SO_4	-11.19	-	Welch *et al.* (2008)
K-Jarosite	3.88	298	H_2SO_4	-10.80	-	Welch *et al.* (2008)

(1) Average rate based on K release, as explained in the text; (2) Ultrapure water (18 MΩ·cm); (3) pH and rate values estimated from plots

Table 1

pH	T(K)	Solution type	Alunite	Al(OH)$_3$(a)	Felsobanyaite	Diaspore	Gibbsite
2.9	280	H$_2$SO$_4$	-9.78	-8.17	-16.40	-4.16	-5.30
2.9	293	H$_2$SO$_4$	-8.03	-7.27	-16.51	-3.32	-4.53
3.2	312	H$_2$SO$_4$	-3.15	-5.12	-13.13	-1.26	-2.55
3.9	293	H$_2$SO$_4$	-3.51	-4.20	-7.03	-0.26	-1.47
4.6	280	DDW[1]	-2.93	-3.31	-1.65	0.69	-0.45
4.8	294	DDW[1]	-1.11	-2.05	-1.07	1.89	0.68
7.0	293	Tris buffer	-0.97	-0.31	2.23	3.64	2.43
7.8	279	Tris buffer	-4.19	-0.57	3.08	3.44	2.30
8.0	294	Tris buffer	-3.39	-0.30	0.21	3.64	2.42
8.0	313	Tris buffer	-4.88	-0.58	-5.44	3.28	1.98

Saturation indices at the end of the experiments. For the calculations, the largest concentrations achieved in any of the replicate experiments for each set of conditions has been selected. [1] DDW corresponds to double distilled water.

Table 2

pH	T(K)	$\%Al^{3+}$	$\%AlOH^{2+}$	$\%Al(OH)_2^+$	$\%Al(OH)_4^-$	$\%AlSO_4^+$	$\%K^+$	$\%HSO_4^-$	$\%SO_4^{2-}$
2.9	280	51	0	0	0	48	100	8	89
2.9	293	49	0	0	0	50	100	10	87
3.2	312	42	1	0	0	56	100	9	81
3.9	293	81	5	0	0	14	100	1	94
4.6	280	85	10	1	0	4	100	0	98
4.8	294	59	28	10	0	3	100	0	99
7	293	0	0	5	90	0	100	0	100
7.8	279	0	0	1	99	0	100	0	100
8	294	0	0	0	99	0	100	0	100
8	313	0	0	0	100	0	100	0	100

Table 3

Surface	Optimised surface energy in vacuo (J/m^2)	Optimised surface energy solvated (J/m^2)
(003) shift 0.0000	0.511	0.286
(003) shift 0.5000	0.685	0.679
(10-2) shift 0.2435	1.218	1.077
(10-2) shift 0.7565	0.818	0.784
(1-12)	1.006	0.884
(1-1-1) termination 1	0.966	0.926
(1-1-1) termination 2	0.839	0.786
(10-1)	1.105	0.968
(2-10)	0.861	0.814

Table 4

Buckingham

Interaction	A (eV)	ρ (Å)	C(eVÅ^6)
K – O1	1080.992	0.30	0.0
K – O2	1250.666	0.30	0.0
Al – O1	529.74758	0.29912	0.0
Al – O2	900.52479	0.29912	0.0
H – O1	102.2763	0.25	0.0
H – O2	161.8440	0.25	0.0
O1 – O1	103585.02	0.2	25.98
O1 – O2	103585.02	0.2	25.98
O2 – O2	103585.02	0.2	25.98

Morse

Interaction	D (eV)	a (Å^{-1})	r_0 (Å)
S – O1	5.0	1.2	1.515
H – O2	7.0525	2.1986	0.9685

Three-body

Interaction	k (eV.rad^{-2})	θ_0 (º)
O1 – S – O1	15.0	109.47

Table S1 (Electronic Supplementary Material)

Figures
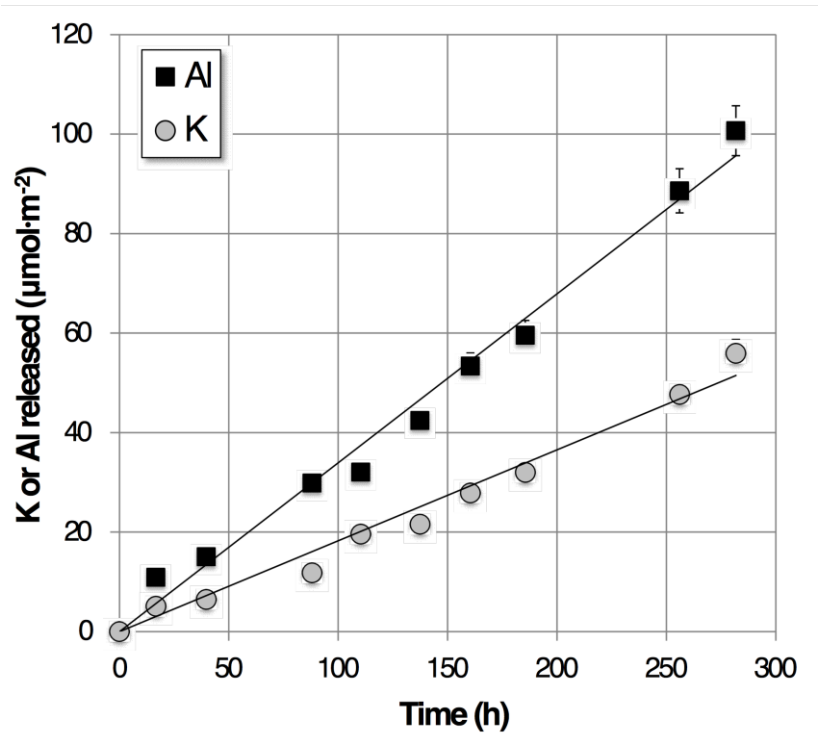
Figure 1
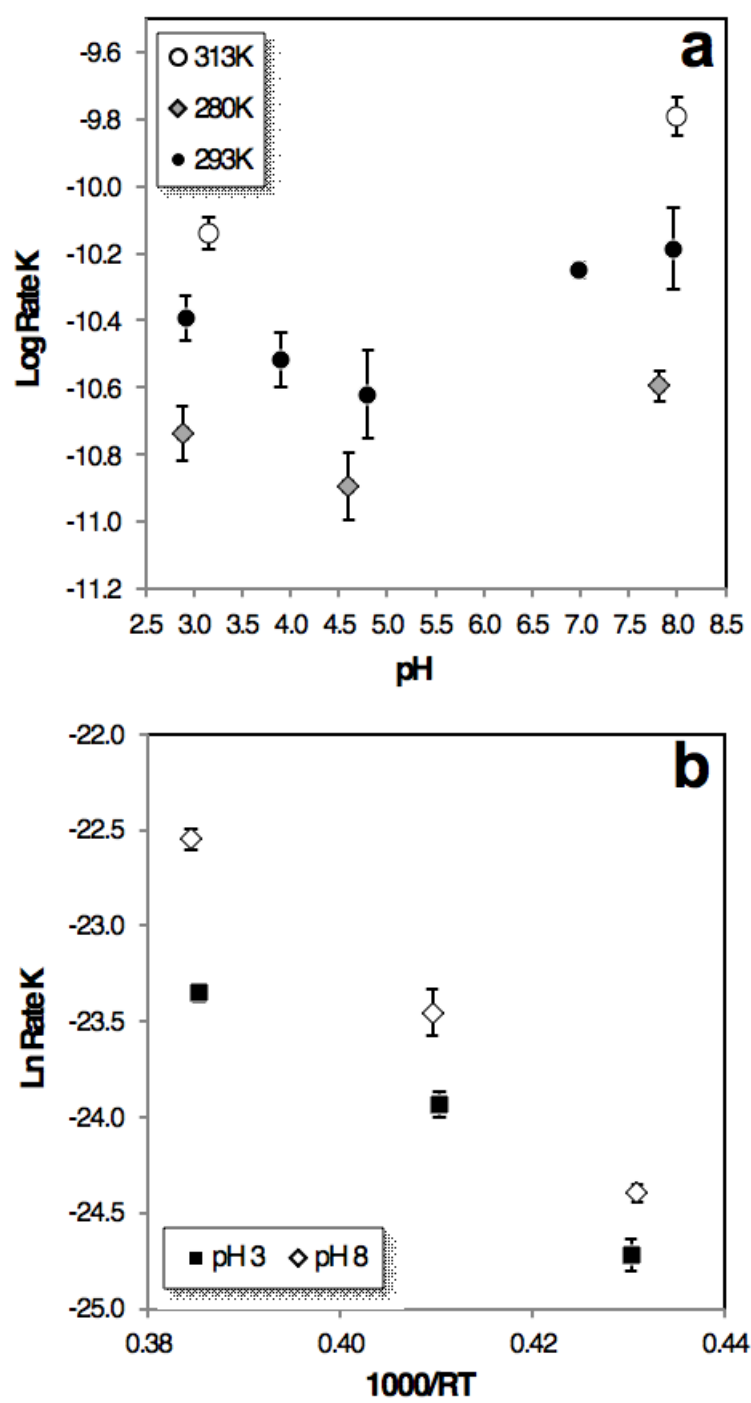
Figure 2
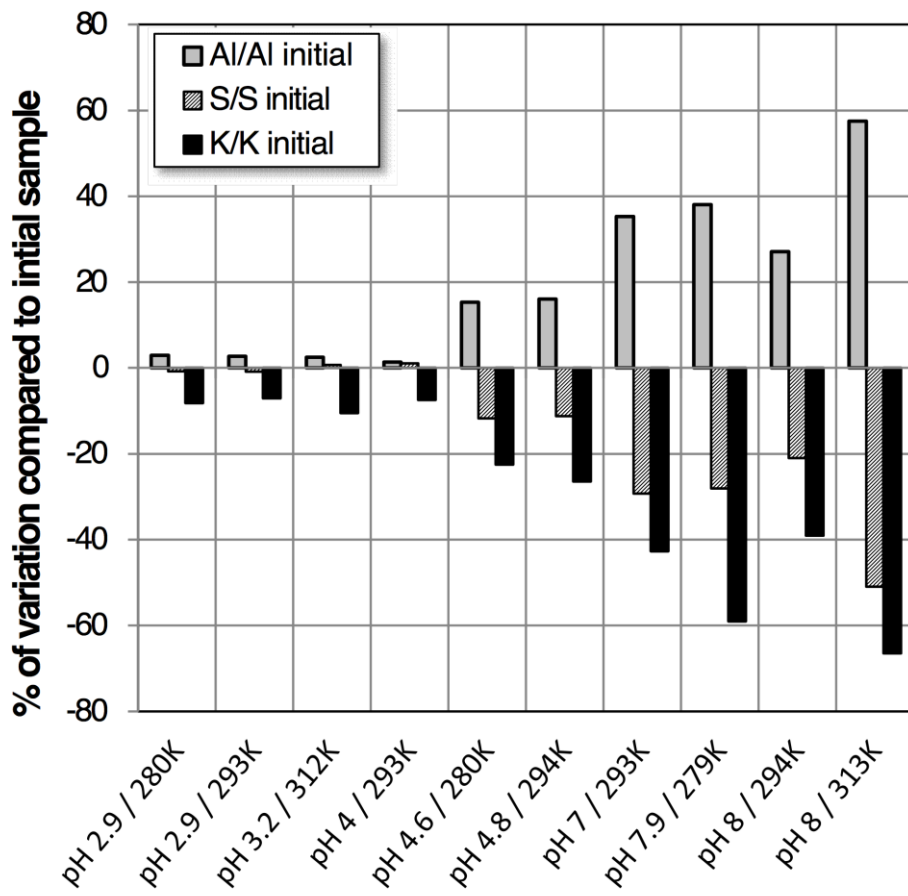
Figure 3
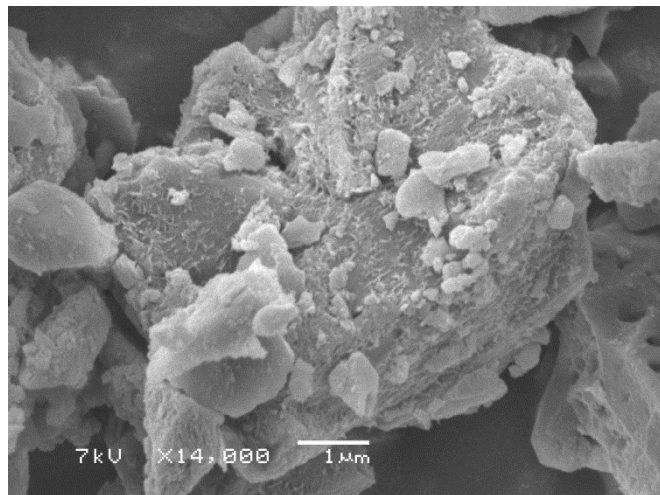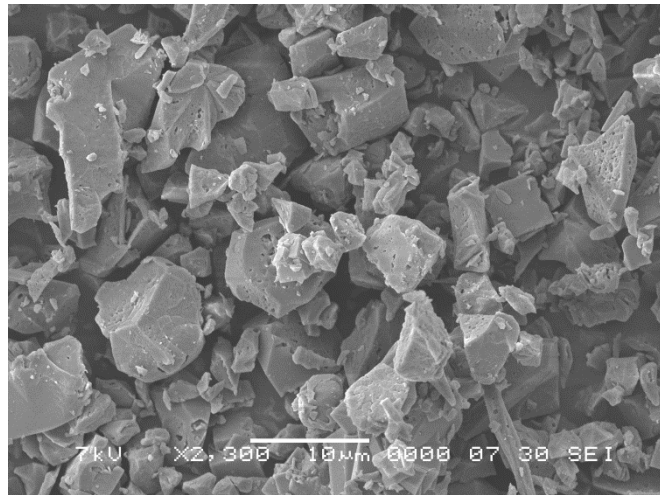
Figure 4

Figure 5

Figure 6